Electroreduction of $Pd_2(dppm)_2Cl_2$ and $Pd(dppm)Cl_2$ [dppm = bis(diphenylphosphino)methane] in aprotic medium under carbon dioxide: electrogeneration of $Pd_3(\mu_3\text{-}CO)(\mu\text{-}dppm)_3$

Isabelle Gauthron,[a] Yves Mugnier,*[,a] Karine Hierso[b] and Pierre D. Harvey*[,b]

[a] *Laboratoire de Synthèse et d'Électrosynthèse Organométalliques (CNRS UMR 5632), Faculté des Sciences Gabriel, Université de Bourgogne, 21000 Dijon, France*
[b] *Département de Chimie, Université de Sherbrooke, J1K 2R1 Sherbrooke, Québec, Canada*

The electroreduction of the d^9–d^9 $Pd_2(dppm)_2Cl_2$ and monomeric d^8 $Pd(dppm)Cl_2$ complexes in aprotic medium (such as DMF, THF and acetonitrile) has been performed under CO_2 atmosphere. In all cases the final products are CO_3^{2-} anion, CO and the neutral $Pd_3(\mu_3\text{-}CO)(\mu\text{-}dppm)_3$ cluster. This electroreduction is not catalytic but rather stoichiometric. The electroreduction mechanisms have been addressed experimentally by electrochemical methods and IR spectroscopy, and theoretically by density functional methods *via* the geometry optimizations of the proposed intermediates. The intermediates "$Pd_2(dppm)_2$" and "Pd(dppm)" are assumed to be active towards the binding of CO_2 prior to its reduction.

Électroréduction de $Pd_2(dppm)_2Cl_2$ et de $Pd(dppm)Cl_2$ [dppm = bis(diphénylphosphino)méthane] en milieu aprotique sous dioxyde de carbone: Électrogénération de $Pd_3(\mu_3\text{-}CO)(\mu\text{-}dppm)_3$. L'électroréduction du complexe d^9-d^9 $Pd_2(dppm)_2Cl_2$ et du monomère d^8 $Pd(dppm)Cl_2$ en milieu aprotique (DMF, THF et acétonitrile) a été effectuée sous atmosphère de CO_2. Dans tous les cas les produits finaux sont l'anion CO_3^{2-}, CO et le cluster neutre $Pd_3(\mu_3\text{-}CO)(\mu\text{-}dppm)_3$. Cette électroréduction n'est pas catalytique mais stoechiométrique. Les mécanismes d'électroréduction ont été étudiés expérimentalement par des méthodes électrochimiques et par spectroscopie IR, et théoriquement par les méthodes de la fonctionnelle de la densité via les optimisations géometriques des intermédiaires proposés. Les intermédiaires "$Pd_2(dppm)_2$" et "Pd(dppm)" sont supposés être actifs vis à vis de la fixation du CO_2 avant sa réduction.

The transformation of carbon dioxide into useful chemical derivatives constitutes an attractive goal in the field of chemistry. In this way the electrochemical reduction of CO_2 has been noted as one practical method.[1] Its reduction into its anion radical requires quite a negative potential,[2] and a dependence on both the nature of the electrode and the reaction medium has been observed in the products. Considerable efforts have been made to find catalysts that allow a substantial decrease of the CO_2 reduction potential and provide product selectivity.[3,4] The most extensively studied homogeneous catalysts so far are transition-metal complexes containing either macrocyclic or bipyridine ligands.[5] Only a few reports have appeared describing the electrochemical reduction of CO_2 using transition-metal phosphine complexes.[6–10] Recently DuBois and coworkers showed that [Pd(triphosphine)(solvent)]$(BF_4)_2$ complexes can exhibit high catalytic rates for the electrochemical reduction of CO_2 at relatively positive potentials.[5,8,10] More recently, these authors reported that the complex $Pd_2(CH_3CN)_2(eHTP)(BF_4)_4$, where eHTP is bis[bis(diethylphosphino)ethyl]phosphinomethane, catalyses the electrochemical reduction of CO_2 to CO in acidic dimethylformamide solution.[10d] In this paper we report the electrochemical behavior of $Pd_2(dppm)_2Cl_2$ and $Pd(dppm)Cl_2$ in the presence of carbon dioxide [dppm = bis(diphenylphosphino)methane]. During the course of this study, the geometry of some of the proposed key intermediates has been optimized using density functional theory, in order to obtain information regarding their structures and the mechanism of CO_2 activation.

Experimental

Materials

$Pd_2(dppm)_2Cl_2$[11a] and $Pd_2(dppm)_3$[11b] have been prepared according to literature procedures. $Pd(dppm)Cl_2$: $PdCl_2$ (Aldrich; 0.52 g, 2.9×10^{-3} M) and dppm (Aldrich; 1.14 g, 2.9×10^{-3} M) were suspended in 50 ml of ethanol (95%) and 50 ml of conc. HCl. The solution was heated to reflux for a period of four hours. A white precipitate with a yellow solution was obtained. The solution was filtered and the white solid was washed with 50 ml of water and 50 ml of ethanol. Yield 89%. The identity of the product was verified by ^1H NMR spectrometry and chemical analysis.

IR measurements

All IR measurements were performed on a Nicolet 205 spectrophotometer. The electrolysis solutions were transferred into an air-tight IR cell *via* canular techniques. No attempt to isolate the palladium species was made.

Electrochemistry

All manipulations were performed using standard Schlenk techniques in an atmosphere of dry, oxygen-free, nitrogen or argon gases. Tetrahydrofuran was distilled under argon from sodium and benzophenone. Acetonitrile (ACN) was purified by simply passing the solvent through a column packed with alumina previously dried at 120 °C; it was deoxygenated by argon bubbling immediately before use. The supporting electrolytes were 0.2 M $(Bu^n)_4NPF_6$ or LiCl, which were dried and degassed before use. In cyclic voltammetry experiments,

the concentration of $Pd_2(dppm)_2Cl_2$, $Pd(dppm)Cl_2$ or $Pd_2(dppm)_3$ was nearly 10^{-3} M. Voltammetry analyses were carried out in a standard three-electrode cell with a Tacussel UAP4 unit cell. The reference electrode was a saturated calomel electrode separated from the solution by a sintered glass disk. The auxiliary electrode was a platinum wire. For all voltammetric measurements the working electrode was a vitreous carbon electrode. The controlled potential electrolyses were performed with an Amel 552 potentiostat coupled to an Amel 721 electronic integrator. High scale electrolysis was performed in a cell with three compartments separated with fritted glasses of medium porosity. A carbon gauze was used as the cathode, a platinum plate was used as the anode and a saturated calomel electrode was used as the reference electrode. For thin layer cyclic voltammetry the vitreous carbon electrode was lowered until contact with the flat floor of the electrolytic scale cell so that only a thin layer of solution existed between them.

Computational details

The reported density functional calculations were all carried out utilizing the Amsterdam Density Functional (ADF) program developed by Baerends *et al.*[12,13] and vectorized by Raveneck.[14] The numerical integration procedure applied for the calculations was developed by te Velde and coworkers.[15] The geometry optimization procedure was based on the method developed by Versluis and Ziegler.[16] The electronic configurations of the molecular systems were described by an uncontracted double-ζ basis set[17] on palladium for the 4s, 4p and 5s orbitals, and triple-ζ for the 5d ones. Double-ζ STO basis sets[18] were used for phosphorous (3s, 3p), oxygen (2s, 2p), carbon (2s, 2p), and hydrogen (1s) orbitals, augmented with a single 4d polarization function for P, a single 3d one for O and C, and a 2p function for H. No polarization function was used for palladium. The $1s^2 2s^2 2p^6 3s^2 3d^{10}$ configuration on palladium, the $1s^2 2s^2$ configuration on phosphorous, and the $1s^2$ configurations on oxygen and carbon were treated by the frozen-core approximation.[13] A set of auxiliary[19] s, p, d, f and g STO functions, centered on all nuclei, was used in order to fit the molecular density and present Coulomb and exchange potentials accurately in each SCF cycle. Energy differences were calculated by including the local exchange-correlation potential of Vosko *et al.*[20] No non-local exchange or correlation corrections were made for the geometry optimizations.

Results and Discussion

Electrochemistry

We have examined the electrochemical behavior of $Pd_2(dppm)_2Cl_2$ **1** and $Pd(dppm)Cl_2$ **2** in aprotic medium. The thin layer cyclic voltammogram of **1** at 0.02 V s^{-1} in tetrahydrofuran (THF) solution containing 0.2 M $(Bu^n)_4NPF_6$ as supporting electrolyte on a vitreous carbon electrode and at room temperature exhibits a strong reduction peak (D) around −1.2 V *vs.* SCE. The return potential scan reduction peak D exhibits two oxidation peaks O_1 and O_2 [D, E_p = −1.23 V; O_1, E_p = −0.47 V; O_2, E_p = −0.16 V *vs.* saturated calomel electrode (SCE); see Table 1, entry 1]. In diffusion, at 0.1 V s^{-1}, a similar cyclic voltammogram is obtained except that O_2 appears as a shoulder. O_1 and O_2 correspond to the oxidation of Pd^0 complexes. In particular O_2 is the oxidation peak of the known $Pd_2(dppm)_3$ complex **4**, based upon comparison with an authentic sample.

Peak O_1, which is situated at a lower anodic potential than peak O_2, probably corresponds to the oxidation of an anionic Pd^0 complex **3** formulated as $Pd_2(dppm)_2Cl_x^{x-}$. Amatore *et al.* showed that anionic Pd^0 species such as $[Pd^0(PPh_3)_2Cl_x]_n^{(nx)-}$ can be obtained by electroreduction of $PdCl_2(PPh_3)_2$ in the absence of PPh_3.[21] To obtain further proof of the formation of **3** we have examined the electrochemical behavior of **1** in DMF containing 0.2 M LiCl as supporting electrolyte salt. The cyclic voltammogram of **1** exhibits peaks D and O_1; only a shoulder appears at the potential of peak O_2 (see Table 1, entry 7). This result indicates that an anionic species formulated as $Pd_2(dppm)_2Cl_x^{x-}$ is relatively stable on the cyclic voltammetry timescale; but under these conditions when an electrolysis is performed at the potential of peak D at 0 °C (see Table 2, entry 1), the two oxidation peaks O_1 and O_2 are observed from the electrolyzed solution. Increasing the temperature from 0 °C to 20 °C causes peak O_1 to decrease and peak O_2 to increase (Fig. 1).

The above results are in accordance with the following two reactions:

$$\underset{\mathbf{1}}{Pd_2(dppm)_2Cl_2} + 2e^- \rightarrow \underset{\mathbf{3}}{Pd_2(dppm)_2Cl_x^{x-}} + (2-x)\ Cl^- \quad (1)$$

$$2\ \underset{\mathbf{3}}{Pd_2(dppm)_2Cl_x^{x-}} \rightarrow \underset{\mathbf{4}}{Pd_2(dppm)_3} + \text{“}Pd_2(dppm)Cl_x^{x-}\text{”} + x\ Cl^- \quad (2)$$

The two-electron reduction of **1** gives the anionic species **3**, which evolves into a mixture of **4** and an unsaturated derivative of Pd^0 formulated as “$Pd_2(dppm)Cl_x^{x-}$”. This latter is found to be very unstable within the timescale of the cyclic voltammogram [*i.e.* “$Pd_2(dppm)Cl_x^{x-}$” decomposes]. Furthermore the addition at 0 °C of dppm to the electrolyzed solution containing **3** and **4** causes peak O_1 to disappear completely and peak O_2 to appear according to the reaction (3):

$$\underset{\mathbf{3}}{Pd_2(dppm)_2Cl_x^{x-}} + dppm \rightarrow \underset{\mathbf{4}}{Pd_2(dppm)_3} + x\ Cl^- \quad (3)$$

As mentioned above, the formulated species **3** is relatively unstable on the timescale of the electrolysis so that no NMR spectroscopy experiment was possible.

In DMF containing $(Bu^n)_4NPF_6$ or LiCl as supporting electrolyte the cyclic voltammogram of **1** is not modified in the presence of added Br^- ion (as Bu_4NBr), showing either that the halogen-exchange reaction from **3** does not occur, or that the exchange occurs but the voltammograms of the chloro and bromo derivatives are the same.

If CO_2 is bubbled through the solution, a well defined A_1/A'_1 system appears in thin layer voltammetry after several

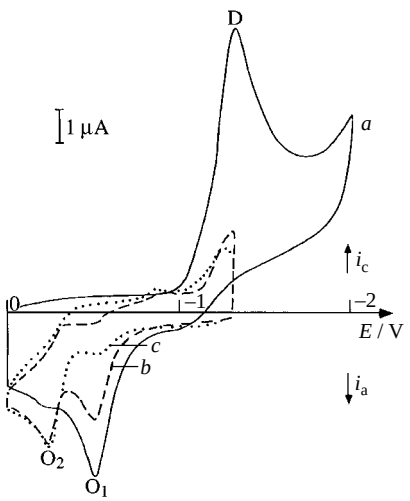

Fig. 1 Cyclic voltammogram of **1** in DMF/0.2 M LiCl solution: *a* initial voltammogram; *b* after two-electron reduction of **1** at −1.3 V at 0 °C; *c* after evolution at room temperature. Starting potential: 0 V for *a*, −1.3 V for *b* and *c*; sweep rate: 0.2 V s^{-1}

Table 1 Electrochemical data for palladium complexes

Entry	Complex	Solvent/ electrolyte salt	Sweep rate/ V s^{-1}	Oxidation peak/V[a]	Reduction peak/V[a]
1	**1**	THF/Bu_4NPF_6	0.02[b]	O_1 −0.47	D −1.23
				O_2 −0.16	
2	**1**	THF/Bu_4NPF_6[c]	0.02[b]	O_1 −0.50	D −1.21
				O_2 −0.16	
				A'_1 −0.59	A_1 −0.79
3	**1**	ACN/Bu_4NPF_6	0.02[b]	O_1 −0.35	D −0.89
				O_2 −0.16	
4	**1**	ACN/Bu_4NPF_6[c]	0.02[b]	O_1 −0.35	D −0.89
				O_2 −0.15	
				A'_1 −0.65	A_1 −0.70
5	**1**	DMF/Bu_4NPF_6	0.02[b]	O_1 −0.53	D −1.18
				O_2 −0.14	
6	**1**	DMF/Bu_4NPF_6[c]	0.02[b]	O_1 −0.52	D −1.20
				O_2 −0.24	
				A'_1 −0.59	A_1 −0.72
7	**1**	DMF/LiCl	0.2	O_1 −0.50	D −1.32
				O_2 −0.20	
8	**7**	ACN/Bu_4NPF_6[c]	0.1	B′ −1.40	B −1.56
9	**7**	THF/Bu_4NPF_6[c]	0.02[b]	B'_1 −1.18	B_1 −1.29
				B'_2 −1.39	B_2 −1.52
				A'_1 −0.59	A_1 −0.76
10	**4**	THF/Bu_4NPF_6	0.1	O_2 −0.12	R −0.48
11	**4**	DMF/Bu_4NPF_6	0.1	O_2 −0.10	R −0.48
12	**2**	THF/Bu_4NPF_6	0.02[b]	O'_1 −0.58	R_1 −1.23
				O'_2 −0.23	
				O'_3 +0.04	
13	**2**	THF/Bu_4NPF_6[c]	0.02[b]	O'_1 −0.58	R_1 −1.19
				O'_2 −0.22	
				O'_3 +0.04	A_1 −0.76
				A'_1 −0.60	
14	**2**	ACN/Bu_4NPF_6	0.02[b]	O'_1 −0.73	R_1 −1.00
				O'_2 −0.34	
				O'_3 +0.03	
15	**2**	ACN/Bu_4NPF_6[c]	0.02[b]	O'_1 −0.73	R_1 −1.00
				O'_2 −0.34	
				O'_3 +0.03	A_1 −0.71
				A'_1 −0.66	
16	**13**	ACN/Bu_4NPF_6[c]	0.02[b]	A'_1 −0.68	B* −1.60

[a] Vitreous carbon electrode is used as working electrode. [b] In thin layer voltammetry. [c] Under carbon dioxide.

potential scans (Fig. 2), while the intensities of the oxidation peaks O_1 and O_2 and the reduction peak D decrease (A_1, $E_p = -0.79$ V; A'_1, $E_p = -0.59$ V *vs.* SCE; see Table 1, entry 2; the $i_{pA'_1}/i_{pA_1}$ ratio of the system remains unity). The A_1/A'_1 system is indicative of the presence of $Pd_3(\mu_3\text{-CO})(\mu\text{-dppm})_3$ **5**.[22]

Under these conditions, the bulk electrolysis of **1** at −1.6 V, under CO_2 at room temperature, leads to solution colour changes from orange to brown after consumption of over four equivalents of electrons ($n_{exp} = 4.17$ F mol^{-1}; see Table 2, entry 2). In cyclic voltammetry of the resulting solution, the oxidation peaks A'_1 and O_2 appear during the anodic scan. If the potential scan is reversed after peak O_2, two reduction peaks A_1 and D are observed. Peak D is found only if the potential is reversed after peak O_2. We have noted that the intensity of peak O_2 relative to that of peak A'_1 decreases when the temperature increases. In the presence of added dppm, the relative intensity of peak O_2 increases (*vide infra*).

Table 2 Controlled potential electroreductions of palladium complexes on a carbon gauze electrode

Entry	Complex	Solvent/ electrolyte salt	T	E/V *vs.* SCE	n_{exp}/ F mol^{-1}	Solution colour
1	**1**	DMF/LiCl	0 °C	−1.30	1.84	red
2	**1**	THF/Bu_4NPF_6[a]	r.t.	−1.60	4.17	brown
3	**1**	ACN/Bu_4NPF_6[a]	r.t.	−1.60	4.25	brown
4	**1**	ACN/Bu_4NPF_6[a]	r.t.	−1.15	2.03	green
5	**1**	THF/Bu_4NPF_6[a]	r.t.	−1.30	2.08	green
6	**1**	THF/Bu_4NPF_6	r.t.	−1.20	2.05	brown
7	**2**	ACN/Bu_4NPF_6[a]	r.t.	−1.60	3.78	brown
8	**2**	ACN/Bu_4NPF_6[a]	r.t.	−1.20	1.90	brown
9	**13**	ACN/Bu_4NPF_6[a]	r.t.	−1.60	1.60	brown
10	**2**	THF/Bu_4NPF_6[a]	r.t.	−1.05	1.95	brown
11	**2**	THF/Bu_4NPF_6[a]	r.t.	−1.60	3.95	brown

[a] Under CO_2.

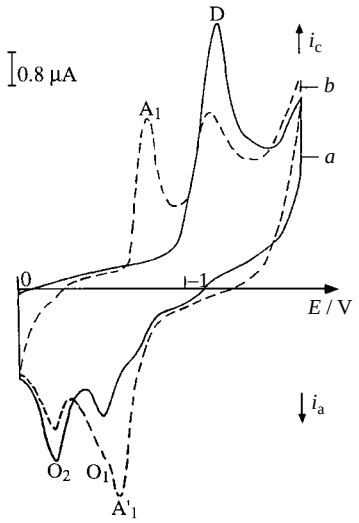

Fig. 2 Thin layer cyclic voltammogram of **1** in THF/0.2 M $(Bu^n)_4NPF_6$ solution under CO_2: *a* first scan; *b* after several scans. Starting potential: 0 V; sweep rate: 0.02 V s^{-1}

Voltammograms similar to those of Fig. 2 are obtained in acetonitrile (ACN) or dimethylformamide (DMF) solutions containing 0.2 M $(Bu^n)_4NPF_6$ as supporting electrolyte starting from **1**; the A_1/A'_1 system is also observed in thin layer voltammetry during the second scan.

When a bulk electrolysis of **1** is performed at −1.6 V in the presence of carbon dioxide in ACN or DMF solution, the cyclic voltammogram of the resulting solution also exhibits the A_1/A'_1 system. In IR spectroscopy a ν_{CO} band at 2358 cm^{-1} appears, which is characteristic of the presence of free carbon monoxide in the electrolyzed solution, based on the observation that a DMF solution containing CO exhibits the same band. The addition of $BaCl_2$ water solution to the electrolyzed solution of **1** in ACN/0.2 M $(Bu^n)_4NPF_6$ causes $BaCO_3$ to precipitate. After appropriate workup, $BaCO_3$ has been collected and identified by its IR spectrum.

As recently mentioned,[22] the A_1/A'_1 system corresponds to the neutral cluster $Pd_3(\mu_3\text{-CO})(\mu\text{-dppm})_3$ **5**, as verified with an authentic sample of $Pd_3(\mu_3\text{-CO})(\mu\text{-dppm})_3^{2+}$. The dicationic cluster has been initially prepared from palladium(II) acetate with dppm and CO in aqueous acetone containing an excess of trifluoroacetic acid according to the following literature reaction:[23]

$$3\ Pd(OAc)_2 + 3\ dppm + 3\ CO + H_2O + 2\ CF_3CO_2H \rightarrow Pd_3(\mu_3\text{-CO})(\mu\text{-dppm})_3(O_2CCF_3)^+ + CF_3CO_2^- + 2\ CO_2 + 6\ AcOH \quad (4)$$

The mechanism of formation of this cluster has recently been fully investigated by Puddephatt *et al.*[24]

Thus, these results show that the electrochemical reduction of **1** at a potential of −1.6 V in aprotic medium and in the presence of carbon dioxide yields CO_3^{2-}, carbon monoxide and the neutral cluster $Pd_3(\mu_3\text{-CO})(\mu\text{-dppm})_3$ **5**, according to the following global reaction:

$$3\ \underset{\mathbf{1}}{Pd_2(dppm)_2Cl_2} + 6\ CO_2 + 12\ e^- \rightarrow 2\ \underset{\mathbf{5}}{Pd_3(dppm)_3CO} + 6\ Cl^- + 3\ CO_3^{2-} + CO \quad (5)$$

5 is then oxidized to the dicationic derivative $Pd_3(\mu_3\text{-CO})(\mu\text{-dppm})_3^{2+}$:

$$\underset{\mathbf{5}}{Pd_3(dppm)_3CO} - 2\ e^- \rightleftharpoons Pd_3(dppm)_3CO^{2+}$$

A_1/A'_1 system (6)

In all cases, we have verified that the cyclic voltammogram of $Pd_3(\mu_3\text{-CO})(\mu\text{-dppm})_3^{2+}$ was not modified in the presence of carbon dioxide.[25]

To gain more insight into the electroreduction process, in particular into the formation of the cluster, we have performed the electrolysis of **1** in the presence of carbon dioxide at potentials higher than −1.6 V in ACN or THF solution containing $(Bu^n)_4NPF_6$ as supporting electrolyte. The bulk electrolysis of **1** in the presence of carbon dioxide at −1.15 V in ACN/$(Bu^n)_4NPF_6$ solution, resulted, after consumption of about two equivalents of electrons (n_{exp} = 2.03 F mol^{-1}; see Table 2, entry 4), in a green solution containing complex **7**. The latter exhibits a different cyclic voltammogram as shown in Fig. 3. If the potential scan is reversed after peak B, two oxidation peaks B′ and A'_1 appear. In thin layer voltammetry, the A_1/A'_1 system becomes well defined after several potential scans. As this green solution is only stable under a CO_2 atmosphere, no IR spectroscopic study is possible.

When the electrolysis of **1** is performed at the peak potential D in THF/$(Bu^n)_4NPF_6$ solution, *i.e.* at −1.3 V, under CO_2, after consumption of about two equivalents of electrons (n_{exp} = 2.08 F mol^{-1}; see Table 2, entry 5) the cyclic voltammogram of the green solution obtained and containing complex **7** exhibits two reduction peaks B_1 and B_2 at −1.29 V and −1.52 V *vs.* SCE, respectively (see Table 1, entry 9). When the potential is reversed after peak B_2, two oxidation peaks B'_2 and B'_1 appear at −1.18 V and −1.39 V *vs.* SCE, respectively (Fig. 4).

We can postulate that the initial step corresponds to the formation of a Pd^0 complex $Pd_2(dppm)_2$ **6**, which is formed from the electrogenerated species **3** and **4** according to the two

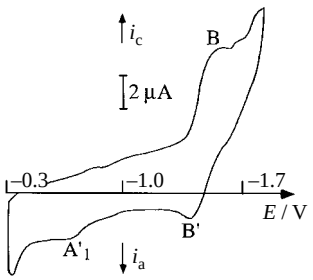

Fig. 3 Cyclic voltammogram of **1** in ACN/0.2 M $(Bu^n)_4NPF_6$ solution after two-electron reduction at −1.15 V under CO_2. Starting potential: −0.3 V; sweep rate: 0.1 V s^{-1}

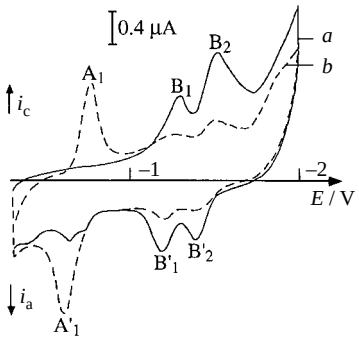

Fig. 4 Thin layer cyclic voltammograms of **1** in THF/0.2 M $(Bu^n)_4NPF_6$ solution after two-electron reduction at −1.3 V under CO_2: *a* first scan; *b* after several scans. Starting potential: −0.2 V; sweep rate: 0.02 V s^{-1}

following equilibrium reactions:

$$\underset{\mathbf{3}}{Pd_2(dppm)_2Cl_x}^{x-} \rightleftharpoons \underset{\mathbf{6}}{Pd_2(dppm)_2} + x\ Cl^- \quad (7)$$

$$\underset{\mathbf{4}}{Pd_2(dppm)_3} \rightleftharpoons \underset{\mathbf{6}}{Pd_2(dppm)_2} + dppm \quad (8)$$

As the cyclic voltammetric O_1 peak disappears and the O_2 peak decreases in intensity in the presence of carbon dioxide, we can suggest that the equilibrium reactions (7) and (8) are shifted to the right and the unsaturated electrogenerated Pd^0 complex **6** reacts immediately with CO_2 to give complex **7**, formulated as $Pd_2(dppm)_2(\eta^2\text{-}CO_2)$, according to the following reaction:

$$\underset{\mathbf{6}}{Pd_2(dppm)_2} + CO_2 \rightarrow \underset{\mathbf{7}}{Pd_2(dppm)_2(\eta^2\text{-}CO_2)} \quad (9)$$

This behavior has also been observed by electrolysis. After two-electron reduction ($n_{exp} = 2.05$ F mol^{-1}; see Table 2, entry 6) of **1** in THF/$(Bu^n)_4NPF_6$ solution under argon, derivatives **3** and **4** are obtained. The addition of CO_2 causes peak O_1 to disappear, O_2 to decrease, and B_1 and B_2 to appear.

Recently, the first carbon dioxide coordinated Pd^0 complex $Pd(\eta^2\text{-}CO_2)(PMePh_2)_2$ has been prepared by the reaction of $PdEt_2(PMePh_2)_2$ with methyl acrylate, followed by treatment with CO_2. The characteristic IR bands due to the coordinated CO_2 ligand are observed at 1658 and 1634 cm^{-1}.[26] This complex is air-sensitive and thermally unstable in the presence of CO_2.

The reduction of intermediate **7** in the presence of carbon dioxide gives cluster **5** according to the global reaction:

$$3\ \underset{\mathbf{7}}{Pd_2(dppm)_2(\eta^2\text{-}CO_2)} + 3\ CO_2 + 6\ e^- \rightarrow \underset{\mathbf{5}}{2\ Pd_3(dppm)_3CO} + 3\ CO_3^{2-} + CO \quad (10)$$

The diverse species obtained by electron or CO_2 (or CO_3^{2-}) exchange are represented in Scheme 1. From one species to the other, one electron is exchanged horizontally and one CO_2 molecule (or the related reduced species CO_3^{2-}) vertically.

In order to explain the experimental results we propose that in THF, the uptake of the first electron initially gives the anionic species $Pd_2(dppm)_2(CO_2)^-$ **7′**, which reacts quickly with CO_2 to yield the derivative **8′** (EC process). **8′** is oxidized at the potential of peak B'_1. The uptake of the second electron on **7′** to **7″** is unlikely, so this hypothesis can be ruled out. **8′** is reduced at the potential of peak B_2 to give species **8″**, which is relatively stable on the timescale of the voltammetry experiments. Peak B'_2 corresponds to the oxidation of **8″**.

In ACN/$(Bu^n)_4NPF_6$ solution only one B/B′ system is obtained. We suggest that the intermediate **8′** must be reduced at a lower negative potential than **7**, according to two different

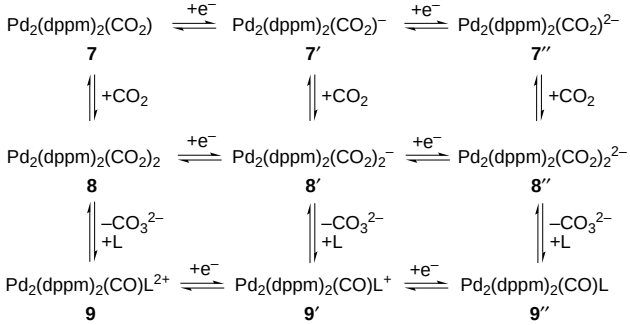

Scheme 1

possibilities (EC mechanism **8′** → **8″** → **9″** or CE mechanism **8′** → **9′** → **9″**). Similar behavior has been observed for palladium[22] and ruthenium[27] complexes exhibiting an associated single-wave two-electron process.

In THF, on the electrolysis timescale (or in cyclic voltammetry at slow sweep rates), complex **8″** evolves with elimination of carbonate ion and formation of the neutral derivative **9″** containing CO as a ligand and probably a donor solvent molecule (L). It is interesting to note that the proposed mechanism (ECEC process) is similar to that of the electrochemical reduction of CO_2 in aprotic medium,[28] giving a mixture of CO and CO_3^{2-} [reaction (11)]:

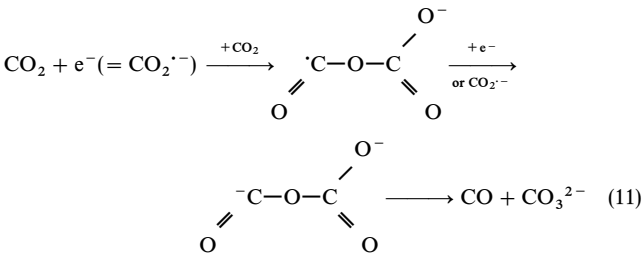

Moreover, the formation of both CO and CO_3^{2-} from the reaction of CO_2 with a transition-metal complex has already been described.[29]

The formation of the neutral cluster **5** from **9″** can be explained by the following reaction:

$$3\ \underset{\mathbf{9''}}{Pd_2(dppm)_2(CO)L} \rightarrow \underset{\mathbf{5}}{2\ Pd_3(dppm)_3CO} + CO + 3\ L \quad (12)$$

Another possibility consists of the reaction between **9″** and **6**:

$$\underset{\mathbf{9''}}{2\ Pd_2(dppm)_2(CO)L} + \underset{\mathbf{6}}{Pd_2(dppm)_2} \rightarrow \underset{\mathbf{5}}{2\ Pd_3(dppm)_3CO} + 2\ L \quad (13)$$

To gain more insight into the electrochemical process, we have examined the behavior of the chemically prepared derivative $Pd_2(dppm)_3$ **4**. The cyclic voltammogram of **4** in a THF/$(Bu^n)_4NPF_6$ solution exhibits an oxidation peak O_2. When the potential scan is reversed after this peak O_2, only one reduction peak R is observed (O_2, $E_p = -0.12$ V; R, $E_p = -0.48$ V *vs.* SCE at 0.1 V s^{-1}; see Table 1, entry 10). Under CO_2 no modification is observed at room temperature. Nevertheless, if the solution of THF containing **4** is heated ($T = 65$ °C) before addition of CO_2, bubbling of carbon dioxide induces disappearance of the oxidation wave O_2 and apparition of the two defined reduction waves B_1 and B_2 by rotating disk electrode (r.d.e.) voltammetry (Fig. 5) according to the reactions (8) and (9). In the presence of an excess of dppm, the equilibrium of reaction (8) is shifted to the left and no further reactivity of **4** is observed in the presence of CO_2, even at high temperatures.

Behavior similar to that of **1** is observed in the case of $Pd(dppm)Cl_2$ **2** in ACN/$(Bu^n)_4NPF_6$ solution. The thin layer

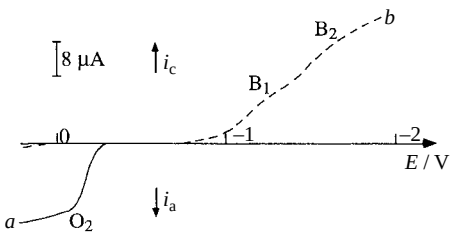

Fig. 5 R.d.e. voltammogram of **4** in THF/0.2 M $(Bu^n)_4NPF_6$ solution: *a* under argon; *b* under CO_2

cyclic voltammogram of **2** in ACN or THF exhibits a strong reduction peak R_1. After reduction at the potential of peak R_1, three oxidation peaks O'_1, O'_2 and O'_3 are observed. The height of peak O'_1 is comparable to that of peak O'_3. After several scans, the intensity of peaks O'_1 and O'_3 decreases and that of peak O'_2 increases. No oxidation peak O_2 is observed, indicating that derivative $Pd_2(dppm)_3$ **4** is not formed during the electroreduction of **2**.

The above results suggest that the anionic species of Pd^0 formulated as $Pd(dppm)Cl_x^{x-}$ **10** is obtained [reaction (14)]. **10** is oxidized in two consecutive steps at the potentials of peaks O'_1 and O'_3 in turn, giving the Pd^I intermediate $Pd(dppm)Cl_x^{(x-1)-}$. On the cyclic voltammetry timescale, **10** evolves to give the neutral Pd^0 derivative formulated as "Pd^0(dppm)L" **11** (L = solvent) [reaction (15)], which is oxidized at the potential peak O'_2.

$$\underset{\mathbf{2}}{Pd(dppm)Cl_2} + 2\ e^- \rightarrow \underset{\mathbf{10}}{Pd(dppm)Cl_x^{x-}} + (2-x)\ Cl^- \quad (14)$$

$$\underset{\mathbf{10}}{Pd(dppm)Cl_x^{x-}} + L \rightleftharpoons \underset{\mathbf{11}}{Pd(dppm)L} + x\ Cl^- \quad (15)$$

In the presence of CO_2, the well defined A_1/A'_1 system is also observed in thin layer voltammetry after several scans if the potential is reversed after peak R_1 (Fig. 6).

The formation of $Pd_3(dppm)_3CO$ **5** from the four-electron reduction of **2** (n_{exp} = 3.78 F mol^{-1}; see Table 2, entry 7) in the presence of CO_2 can be explained by the global reaction:

$$3\ \underset{\mathbf{2}}{Pd(dppm)Cl_2} + 6\ CO_2 + 12\ e^- \rightarrow \underset{\mathbf{5}}{Pd_3(dppm)_3CO} + 6\ Cl^- + 3\ CO_3^{2-} + 2\ CO \quad (16)$$

To gain more insight into the electroreduction process we have performed the electrolysis of **2** in the presence of carbon dioxide at −1.2 V in ACN/$(Bu^n)_4NPF_6$ solution. After consumption of nearly two equivalents of electrons (n_{exp} = 1.90 F mol^{-1}; see Table 2, entry 8), a brown solution containing complex **13** was obtained that exhibits the thin layer cyclic voltammogram in Fig. 7; in the cathodic scan, a well defined reduction peak B* appears (a shoulder is also observed near −0.9 V). When the scan is reversed after peak B*, the oxidation peak A'_1 is again observed (see Table 1, entry 16). Under argon, the height of peak B* decreases and several ill defined oxidation peaks are obtained during the anodic scan.

In IR spectroscopy, bands located at 1696 and 1634 cm^{-1} are observed due to the coordinated CO_2 ligand; as mentioned above, IR bands were observed at 1658 and 1634 cm^{-1} for the first carbon dioxide coordinated Pd^0 complex $Pd(\eta^2\text{-}CO_2)(PMePh_2)_2$.[26] **13** is only stable under CO_2 and isolation causes its decomposition. We suggest that **13** is a derivative

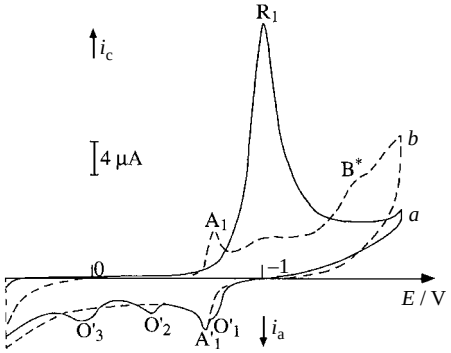

Fig. 6 Thin layer cyclic voltammogram of **2** in ACN/0.2 M $(Bu^n)_4NPF_6$ solution under CO_2: *a* first scan; *b* after several scans. Starting potential: +0.5 V; sweep rate: 0.02 V s^{-1}

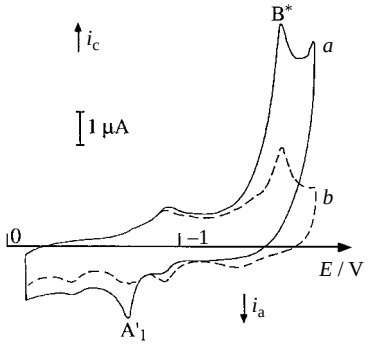

Fig. 7 Thin layer cyclic voltammogram of **2** in ACN/0.2 M $(Bu^n)_4NPF_6$ solution after two-electron reduction at −1.2 V under CO_2: *a* first scan under CO_2; *b* under argon. Starting potential: −0.1 V; sweep rate: 0.02 V s^{-1}

formulated as $Pd(dppm)(\eta^2\text{-}CO_2)$, which is obtained from reaction of CO_2 with the unsaturated Pd^0 intermediate **12** [reaction (19)]; **12** is formed from complexes **10** and **11** by reactions (17) and (18), respectively.

$$\underset{\mathbf{10}}{Pd(dppm)Cl_x^{x-}} \rightleftharpoons \underset{\mathbf{12}}{Pd(dppm)} + x\ Cl^- \quad (17)$$

$$\underset{\mathbf{11}}{Pd(dppm)L} \rightleftharpoons \underset{\mathbf{12}}{Pd(dppm)} + L \quad (18)$$

$$\underset{\mathbf{12}}{Pd(dppm)} + CO_2 \rightleftharpoons \underset{\mathbf{13}}{\text{"}Pd(dppm)(\eta^2\text{-}CO_2)\text{"}} \quad (19)$$

The two-electron reduction of intermediate **13** in the presence of carbon dioxide gives cluster **5**:

$$3\ \underset{\mathbf{13}}{\text{"}Pd(dppm)(\eta^2\text{-}CO_2)\text{"}} + 3\ CO_2 + 6\ e^- \rightarrow \underset{\mathbf{5}}{Pd_3(dppm)_3CO} + 3\ CO_3^{2-} + 2\ CO \quad (20)$$

The two-electron process can be rationalized by a mechanism similar to that described in Scheme 1 with the formation, in the initial step, of the anionic species $Pd(dppm)(\eta^2\text{-}CO_2)^-$.

Similar results are obtained in THF/$(Bu^n)_4NPF_6$ solution. In thin layer cyclic voltammetry, the reduction peak R_1 decreases, the oxidation peaks O'_1, O'_2 and O'_3 disappear while the A_1/A'_1 system appears after several scans (A'_1 is situated at the same potential as O'_1).

When the electrolysis of **2** is performed at −1.6 V in THF/$(Bu^n)_4NPF_6$ solution, cluster **5** is formed after a four-electron reduction (n_{exp} = 3.95 F mol^{-1}; see Table 2, entry 11) of **2** in the presence of CO_2. However, when the electrolysis is performed at −1.05 V, the current drops to zero after consumption of two electrons (n_{exp} = 1.95 F mol^{-1}; see Table 2, entry 10) and no reduction peak is observed by cyclic voltammetry of the resulting solution. In this case, we propose that the equilibrium reactions (18) and (19) are shifted to the left and the electrogenerated species **11** (L = THF) is very unstable on the electrolysis timescale [*i.e.* Pd^0(dppm)L decomposes]. In contrast, when the electrolysis is performed at −1.6 V, the equilibrium reactions are shifted in the opposite way, due to the electrochemical reaction that corresponds to the reduction of **13** [reaction (20)].

The key proposed intermediates in these electrolyses are clearly compounds **6**, **7**, **12** and **13**. They are interesting from a theoretical point of view. For instance, compounds **6** and **7** can exhibit M—M interactions leading to cooperative reactivity. Compounds **8**, **8′** and **8″** can be used as examples where two CO_2 ligands are located near each other. Compound **13** is also important for the preparation of compound **5**. One

important question is: Can compounds **7** and **13** be reduced at low enough potentials to form their corresponding anionic forms? In the next section, these questions will be addressed theoretically using density functional methods (ADF).

Theoretical calculations

Both the experimental and theoretical aspects of the binding of CO_2 on transition metals have been extensively reviewed.[30] Reviews by Gibson[31] and Leitner[32] have also recently appeared. The bonding of CO_2 to a single metal atom can occur *via* two modes: M(η^2-CO_2) and M(η^1-CO_2). Examples of the two types are [Ni(PCy_3)$_2$(η^2-CO_2)][33] and [Ir(dmpe)$_2$Cl(η^1-CO_2)],[34] respectively [Cy = C_6H_{11} and dmpe = {[$(CH_3)_2P$]$_2CH_2$}$_2$]. Calculations reported in the literature[35–40] have focused on four basic bonding modes of CO_2 coordination: (*a*) carbon–oxygen (η^2-CO) "side-on" with C_s symmetry, (*b*) carbon (η^1-C), with C_{2v} symmetry, (*c*) oxygen (η^1-O) "end-on" and (*d*) oxygen–oxygen (η^2-OO) with C_{2v} symmetry. In general, modes *c* and *d* are more energetic than *a* and *b*[31] and will not be dealt with in this work. The binding of CO_2 *via* modes *a* and *b* will now be qualitatively described. CO_2 has 2 sets of orthogonal π molecular orbitals. The bonding interactions between CO_2 and a metal in both modes (η^1 and η^2) takes place *via* two sets of orbitals. The first set involves the in-plane π, *n*π and π* molecular orbitals. The second set involves out-of-plane π, *n*π and π* molecular orbitals. The plane is the M(CO_2) one. The in-plane molecular orbitals are responsible for the major part of the bonding to the transition metal. In the η^1 mode, a significant charge-transfer interaction occurs between the d_{z^2} metal orbital and the π* orbital of CO_2, where the metal acts as a two-electron donor and CO_2 as an acceptor. In opposition, the η^2 mode uses a CO_2 π orbital as the Lewis base (two-electron donor) and an empty d orbital (if available) or a p orbital of the metal atom to generate the σ bond. In this case π back bonding occurs using a filled d_{xz} metal orbital and the empty π* orbital of CO_2. In this work we will concentrate on the η^2 form since experimentally the IR data [ν(CO) = 1696, 1634 cm^{-1}] for **13** indicates the Pd(η^2-CO_2) formulation. Additionally, Salahub and coworkers[40] demonstrated, using ADF in a closely related work, that CO_2 binds a single palladium atom *via* a η^2 coordination mode. In this case the η^1 form was in fact a transition state for the binding of CO_2 to Pd. Furthermore, based upon experience with other related Pd compounds, ADF has proven successful in optimizing geometries.[41,42] For comparison purposes, and to ensure that the calculation methods are adequate for this work, the geometry of the model compound Ni(PH_3)$_2$(η^2-CO_2) was optimized and compared to that of the Ni(PCy_3)$_2$(η^2-CO_2) X-ray structure and to that of the optimized Pd(PH_3)$_2$(η^2-CO_2) compound. We are interested to know what geometry some of the intermediates may have during the various processes encountered in the electroreduction of CO_2. The geometry was restricted to a C_s symmetry (planar), allowing two possible geometries to occur during optimization (η^1-planar, η^2-planar). The geometries converged to the η^2 form for both Ni and Pd (Fig. 8, Table 3).

The comparison of the computed Ni(PH_3)$_2$(η^2-CO_2) and experimental Ni(PCy_3)$_2$(η^2-CO_2) structures is excellent. The largest difference between the two structures is less than 6% [*r*(MP) 2.160 (calcd.) *vs.* 2.294 Å (X-ray)]. The comparison between the calculated and X-ray structure for the Ni(η^2-CO_2) fragment is particularly good with differences not exceeding 2.5%.

We now compare the two optimized geometries for M=Ni and Pd. Both geometries exhibit the same η^2-CO_2 coordination modes with very similar distances and angles. The comparison of the MP, MC and MO indicates that *r*(Ni) < *r*(Pd). This difference is simply due to the difference in covalent radii between Ni and Pd.[43,44] The significant result is that the *r*(CO) distance for the coordinated CO is longer in the Ni case. In addition the ∠ OCO is smaller in the Ni case as well. Knowing that CO_2 activation leads to products in which the hybridization of the C atom changes from sp to sp^2 (carbonate, formate, oxalate, etc. …),[31,32] these calculations predict that the CO_2 geometry in the Ni complex is more distorted than in the Pd one. In other words, the C=O bond is

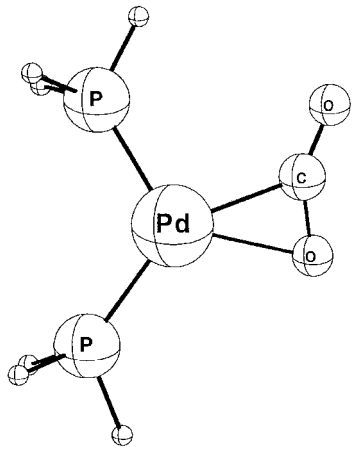

Fig. 8 Optimized geometry of the planar Pd(PH_3)$_2$(η^2-CO_2) model compound. The symmetry was restricted to C_s

Table 3 Comparison of the calculated planar M(PH_3)$_2$(η^2-CO_2) geometries (M = Ni, Pd) and X-ray Ni(PCy_3)$_2$(η^2-CO_2) structures[a]

	Pd(PH_3)$_2$(η^2-CO)$_2$	Ni(PH_3)$_2$(η^2-CO_2)	Ni(PCy_3)$_2$(η^2-CO_2)[b]	Δ[c]
r(MP) long	2.334	2.160	2.294	0.174
r(MP) short	2.249	2.078	2.163	0.171
r(MC)	2.147	1.886	1.857	0.261
r(MO)	2.270	1.921	1.967	0.349
r(CO)	1.191	1.195	1.211	−0.004
r(CO) coordinated	1.215	1.245	1.257	−0.030
∠OCO	151.0	146.0	136.2	
∠OMP	120.1	110.3	105.3	
∠CMP	91.5	97.4	93.9	
∠PMP	116.6	114.1	122.6	
∠CMO	31.7	38.2	38.3	

[a] *r* in Å and ∠ in degrees (°). Only selected data are presented. [b] From ref. 51. [c] Δ is defined as $r(Pd)_{calc} - r(Ni)_{calc}$

weaker in the Ni complex and more likely to be activated in a thermodynamic sense, than the Pd analogue.

The following series of computations concern the reduced "$Pd(dppm)(CO_2)^-$" species, which is generated by the one-electron reduction of compound **13**. The geometry optimizations of the planar $Pd(PH_3)_2(CO_2)^-$ model compounds were performed using the C_s restricted symmetry, and the CO_2 coordination adopted the η^1-bonding form (Fig. 9).

The nature of the frontier orbitals is no different in the reduced and neutral species. HOMO-1 is a bonding interaction between the d_{z^2} mixed with the $d_{x^2-y^2}$ orbital of the metal and the π^* orbital of CO_2. The HOMO is of course singly occupied and is mainly composed of the Pd $5p_z$ orbital (consistent with the $d^{10} + 1\ e^-$ electronic configuration) and the C p_z orbital (along with some significant O p_z orbitals; *i.e.* π^* of the CO_2). The Pd—C interactions are antibonding. The LUMO is the other CO_2 π^* system. As a result, upon reduction of **13**, the reduced species should exhibit an increased Pd—C bond length. The calculated *r*(PdC), *r*(CO) and ∠ OCO data are as follows: 2.177 Å, 1.233 Å and 136.8°, respectively. The increase in *r*(PdC) is indeed computed ($\Delta = +0.030$ Å) but is perhaps not as extensive as one may expect. The reason for this is that the excess electron occupies an orbital that is *delocalized* in the π^* system of the CO_2 fragment. Indeed, *r*(CO) shows an increase from 1.191 and 1.215 Å (average 1.203 Å for the neutral species) to 1.233 Å (charged species; $\Delta \cong 0.030$ Å). The OCO angle decreases greatly from 151.0° to 136.8°. For comparison purposes, *r*(CO) and the OCO angle in acetate ($CH_3CO_2^-$) lie somewhere around 1.24–1.25 Å and 125–130°, respectively. This favorable comparison strongly suggests that CO_2 has become a metallated carboxylate compound (RCO_2^-; R = PdL_2) upon reduction. This observation could explain the reactivity between CO_2^- and CO_2 indicated in reaction (11) (except that CO_2^- is replaced by MCO_2^- here). The computed Pd—P bond lengths, averaging 2.282 Å, are close to that of the neutral species (Table 3; 2.292 Å) but also indicate an increase in Pd—P back bonding (*i.e.* Pd—P bond shortening) due to the increase in electronic density at the metal center upon reduction. The complete computed structures are provided in the Supplementary Material.

The following section addresses the $Pd_2(dppm)_2$ compounds, notably compounds **6**, **7** and **8**. Recently Fink *et al.*[45] pointed out that d^{10} monomeric Pd(diphos) compounds (diphos = diphosphine ligand) are in a monomer–dimer equilibrium. In the dppm case described here, the similarities in the electrolysis of **1** and **2** in the presence of CO_2 is consistent with the literature:

$$2\ Pd(diphos) \rightleftharpoons Pd_2(diphos)_2 \qquad (19)$$

For convenience the starting geometry of **6** was $Pd_2(H_2PCH_2PH_2)_2$ (in a "C_{2v}" restricted symmetry with the methylene groups pointing the same way). The optimizations were performed using the restricted C_s symmetry; this procedure allows some degree of freedom from the molecule. After convergence, the calculated complex does not exhibit a perfectly planar Pd_2P_4 structure. (Fig. 10), but rather the PPdP angles are 168 and 174°. This slight deviation from linearity is due to the fact that the CH_2 groups were placed both pointing the same way instead of in opposite directions (C_{2h} symmetry). This preferred orientation was selected to allow further computations with addition of CO_2 with a minimum of steric effect (see below).

The new feature is, of course, the appearance of Pd···Pd interactions. Here the computed distance is 2.854 Å [*r*(P···P) = 2.956 Å]. The presence of Pd···Pd interactions in d^{10}–d^{10} complexes is well documented in the literature,[46] and can be experimentally addressed by X-ray crystallography (whether there is a chemical bond or just a weak interaction) and by UV-visible and Raman spectroscopy.[46–48] Related examples are Fink's dimer, $Pd_2(Cy_2PCH_2CH_2PCy_2)_2$, $r(Pd_2) = 2.7611$ Å,[45] and $Pd_2(dppm)_3$, reported by Kirss and Eisenberg [$r(Pd_2) = 2.956(1)$ Å[49]]. In this latter case, resonance Raman spectroscopy established that $\nu(Pd_2)$, the Pd_2 stretching frequency, is 120 cm^{-1}. The van der Waals radii is 1.6 Å.[44] Relevant to this work, Sakaki *et al.*[50] have reported a theoretical study on the bond energy and the bonding nature of dinuclear d^{10} metal complexes of the type $(ML_2)_2$ (M = Pd, Pt; L = PH_3), using *ab initio* MO methods. The presence of Pd_2 interactions results from bonding interactions with p_σ orbitals. Also, the HOMO mainly includes the d_σ–d_σ antibonding overlap into which s and p_σ orbitals of one Pd mix in a bonding way with the d_σ orbital of the other Pd atom. Because the d_σ orbital population decreases slightly, and the s orbital population decreases greatly, Sakaki *et al.*[50] concluded that the s and p_σ orbitals mix into the $d_\sigma d_\sigma$ antibonding interaction to reduce the d_σ–d_σ exchange repulsion, and the charge transfer from the d_σ of one M to the sp_σ of the other M is weak. As a consequence, a $sp \rightarrow sp^2$ rehybridization occurs when the geometry changes from the two-coordinate ML_2 system to the three-coordinate $L_2M—ML_2$ one. However, the question is whether the rehybridization process is a complete or partial rehybridization. At a distance of 2.854 Å, which is well above the sum of the covalent radii,[44] it is clear that the rehybridization is not as extensive. Indeed, the calculated Pd—Pd bond energy for $(PH_3)_2Pd—Pd(PH_3)_2$ is rather small (somewhere between 14 and 4 kcal mol^{-1})[50] for a similar distance of ≈2.885 Å (optimized geometry). In conclusion, we should consider the Pd—Pd bonding as weak interactions and

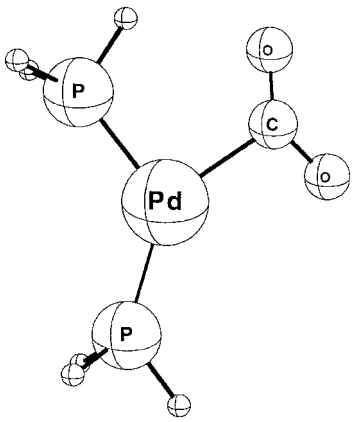

Fig. 9 Optimized geometry of the planar $Pd(PH_3)_2(\eta^1\text{-}CO_2)^-$ model compound. The symmetry was restricted to C_s

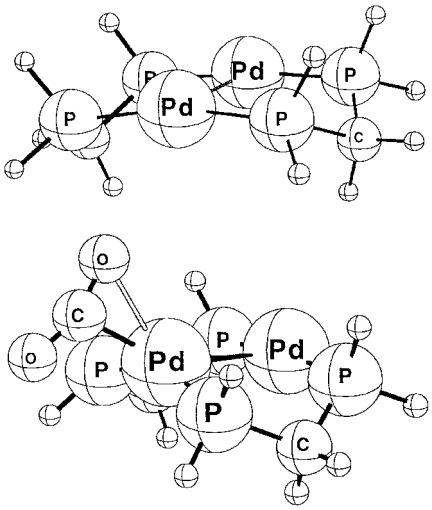

Fig. 10 Optimized geometry of the $Pd_2(H_2PCH_2PH_2)_2$ and $Pd_2(H_2PCH_2PH_2)_2(\eta^2\text{-}CO_2)$ model compounds. The symmetry was restricted to C_s

not as a formal coordination bond. The computed *r*(PdP) data average to 2.262 Å and are normal. For $Pd_2(dppm)_3$, the average X-ray *r*(PdP) is 2.310 Å.[49]

The next point addresses the nature of the cooperation between the two Pd atoms. Compound **7** could exist under a μ-bridging form of the type Pd—O—C(O)—Pd (oxidation of the Pd centers). In prior calculations, the CO_2 was placed in the bridging position with the same distances between Pd—C and Pd—O. The symmetry was restricted to C_s. During the optimization, the CO_2 bridging ligand moved out of its initial bridging position and stabilized in a η^2-conformation (Scheme 2). Here the CO_2 is still behaving as a two-electron donor ligand.

The PdP_2CO conformation is obviously not planar (Fig. 10) as imposed by the computations. Here again some Pd···Pd interactions [$r(Pd_2) = 2.821$ Å, calculated] is also predicted by theory, but does not significantly differ from the model compound $Pd_2(H_2PCH_2PH_2)_2$ described above [$r(Pd_2) = 2.854$ Å]. Other structural data of interest are *r*(PdC), *r*(PdO), *r*(PdP) and the OCO angle: 2.189, 2.579, 2.270 ± 0.015 Å and 151°, respectively (see the Supplementary Material for details). In this case, the Pd—CO_2 bonding is predicted to be slightly weaker in comparison with the data of Table 3 [*i.e.* slightly longer *r*(PdC) and *r*(PdO) values]. The presence of weak Pd···Pd interactions, which induce a localization of part of the electronic density between the two metals, decreases the backbonding interactions between Pd and CO_2. No computation was performed for the reduced species; it is reasonably assumed that the conclusions drawn for the monomeric model compounds discussed above are the same here. We also anticipate that a $Pd(H_2PCH_2PH_2)_2Pd(\eta^2\text{-}CO_2)$ structure with a planar PdP_2CO_2 is also possible, but was not optimized.

The final series of computations deals with compound **8** as regards the nature of the cooperative properties on the $Pd_2(dppm)_2$ skeleton. According to Scheme 1, the conversion of two CO_2 molecules into CO_3^{2-} and CO must pass by a mechanism involving either **8**, **8′** or **8″**. The geometry of **8** was optimized by placing two CO_2 face-to-face (in a restricted C_s symmetry). The optimized geometry (Fig. 11) does keep the face-to-face conformation, but also generates local Pd conformations similar to that shown in Fig. 8.

The *r*(PdC), *r*(PdO), long *r*(PdP), short *r*(PdP) and OCO angle data at convergence are 2.190, 2.284, 2.335 and 2.250 Å and 153.7°, respectively, and compare favorably to that of $Pd(PH_3)_2(\eta^2\text{-}CO_2)$ in Table 3; the Pd—C and Pd—O distances are again slightly longer (same reason: Pd···Pd interactions). The calculated Pd···Pd separation is now

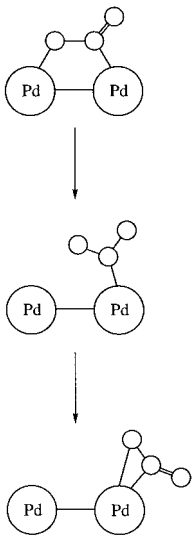

Scheme 2

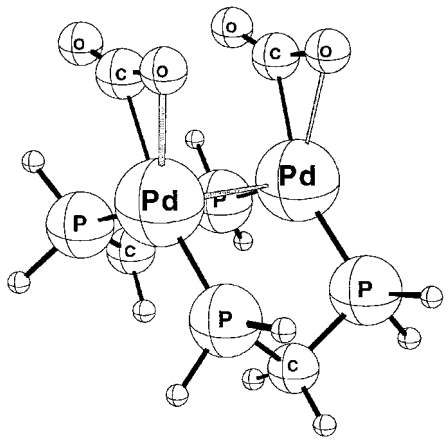

Fig. 11 Optimized geometry of the $Pd_2(H_2PCH_2PH_2)_2(\eta^2\text{-}CO_2)_2$ model compound. The symmetry was restricted to C_s

slightly longer (2.955 Å) but close to that reported for **3**. More importantly, the C···C and O···O contacts (between 3.2 and 3.4 Å) are smaller than the sum of the van der Waals radii.[43] This result predicts that any $CO_2 \cdots CO_2$ intramolecular processes (**8** → **9**, **8′** → **9′**, **8″** → **9″**; Scheme 1) could be possible in a face-to-face geometry. The limiting step now depends upon the relative ratio of CO_2 uptake (ex.: **7** → **8**) *vs.* electron transfer (ex.: **7** → **7′**). These parameters depend upon the applied potential and the CO_2 concentration. The fact that a second metal center is located near the first one allows one to consider the possibility that a second and different molecule can be activated (coordinated) simultaneously. This situation brings in the intramolecular coupling of two different molecules. Monodentate phosphine ligands do not offer this "template" opportunity. The geometry for **8′** and **8″** has not been calculated; it is also anticipated that conclusions similar to those obtained for the planar $Pd(PH_3)_2(CO_2)^-$ model compound will be drawn. The optimized structural data of this compound are also available in the Supplementary Material.

Conclusion

The electroreduction of $Pd_2(dppm)_2Cl_2$ and $Pd(dppm)Cl_2$ in aprotic medium (THF, ACN) under CO_2 leads to $Pd_3(dppm)_3CO$ and CO_3^{2-}. The overvoltage of the CO_2 reduction is decreased by 0.6 V. No catalytic process is observed in these experimental conditions. Studies of this indirect reduction of CO_2 with the above cited palladium derivatives in the presence of added substrates (*i.e.* Lewis acid) are in progress.

Supplementary material

Computed structural data for planar and perpendicular $Pd(PH_3)_2(CO_2)$ and $Pd(PH_3)_2(CO_2)^-$, and for $Pd_2(H_2PCH_2PH_2)_2(CO_2)_x$ ($x = 0, 1, 2$) are available from the authors (8 pages).

Acknowledgements

This research was supported by NSERC (Canada), FCAR (Québec), Électricité de France (EDF—Club d'Électrochimie Organique), the Conseil Régional de Bourgogne and the Préfecture de la Région Bourgogne. We are grateful to Prof. Jean Lessard and Dr. Jean-Marc Chapuzet for helpful discussions.

References

1 (*a*) B. J. Fisher and R. Eisenberg, *J. Am. Chem. Soc.*, 1980, **102**, 7361; (*b*) M. R. M. Bruce, E. Megehee, B. P. Sullivan, H. Thorp, T. R. O'Toole, A. Downard and T. J. Meyer, *Organometallics*, 1988, **7**, 238 and references therein; (*c*) K. W. Frese, D. P. Summers and

M. J. Cinibulk, *J.Electrochem. Soc.*, 1988, **135**, 264; (*d*) C. Amatore and J. M. Savéant, *J. Am. Chem. Soc.*, 1981, **103**, 5021; (*e*) E. Lamy, L. Nadjo and J. M. Savéant, *J. Electroanal. Chem.*, 1977, **78**, 403; (*f*) B. J. Fisher, T. Lehman and E. J. Heitz, *Appl. Electrochem.*, 1981, **11**, 743; (*g*) P. A. Christensen, A. Hammett and A. V. G. Muir, *J. Electroanal. Chem.*, 1990, **288**, 197; (*h*) J. Desilvestro and S. Pons, *J. Electroanal. Chem.*, 1989, **267**, 207.
2 The standard potential of the CO_2/CO_2^- couple in *N*,*N*-dimethylformamide with 0.1 M NEt_4ClO_4 as supporting electrolyte has been estimated to be −2.2 V *vs.* SCE by cyclic voltammetry on a mercury electrode [see ref. 1(*e*)].
3 Recent reviews: (*a*) G. Silvestri, in *Carbon Dioxide as a Source of Carbon*, ed. M. Aresta and G. Forti, NATO ASI Series: Ser. C, Reidel, Dordrecht, 1987, p. 339. (*b*) G. Silvestri, S. Gambino and G. Filardo, in *Enzymatic and Model Carboxylation and Reduction Reactions for CO_2 Utilization*, NATO ASI Series, Reidel, Dordrecht, 1990, **314**, 101.
4 J. P. Collin and J. P. Sauvage, *Coord. Chem. Rev.*, 1989, **93**, 245.
5 D. L. DuBois and A. Miedaner, *J. Am. Chem. Soc.*, 1987, **109**, 113.
6 S. Slater and J. H. Wagenknecht, *J. Am. Chem. Soc.*, 1984, **106**, 5367.
7 A. Szymaszek and F. P. Pruchnik, *J. Organomet. Chem.*, 1987, **376**, 133.
8 D. L. DuBois, A. Miedaner and R. C. Haltiwanger, *J. Am. Chem. Soc.*, 1991, **113**, 8753.
9 K. S. Ratcliff, R. E. Lentz and C. P. Kubiak, *Organometallics*, 1992, **11**, 1986.
10 (*a*) D. L. DuBois and A. Miedaner, *Inorg. Chem.*, 1986, **25**, 4642; (*b*) D. L. DuBois and A. Miedaner, *Inorg. Chem.*, 1988, **27**, 2479; (*c*) A. Miedaner, D. L. DuBois and C. J. Curtis, *Organometallics*, 1993, **12**, 299; (*d*) B. D. Stefey, C. J. Curtis and D. L. DuBois, *Organometallics*, 1995, **14**, 4937.
11 (*a*) L. S. Benner and A. L. Balch, *J. Am. Chem. Soc.*, 1978, **100**, 6099; (*b*) E. W. Stern and K. Maples, *J. Catal.*, 1972, **27**, 120.
12 E. J. Baerends, D. E. Ellis and P. Ros, *J. Chem. Phys.*, 1973, **2**, 41.
13 E. J. Baerends, Ph.D. Thesis, Vrije Universiteit, Amsterdam, 1975.
14 W. Raveneck, in *Algorithms and Applications on Vector and Parallel Computers*, ed. H. J. J. Rigie, Th. J. Dekkor and H. A. van de Vorst, Elsevier, Amsterdam, 1987.
15 P. M. Boerrigter, G. te Velde and E. J. Baerends, *Int. J. Quantum Chem.*, 1988, **33**, 87.
16 L. Versluis and T. Ziegler, *J. Chem. Phys.*, 1988, **88**, 322.
17 (*a*) G. J. Snijders, E. J. Baerends and P. Vernooÿs, *At. Nucl. Data Tables*, 1982, **26**, 483; (*b*) P. Bernooÿs, G. J. Snijders and E. J. Baerends, *Int. Slater Type Basis Functions for the Whole Periodic System*, Free University of Amsterdam, Amsterdam, 1981.
18 (*a*) L. Noodleman and J. G. Norman, *J. Chem. Phys.*, 1979, **70**, 4903; (*b*) L. Noodleman, *J. Chem. Phys.*, 1981, **74**, 5737; (*c*) L. Noodleman and E. J. Baerends, *J. Am. Chem. Soc.*, 1984, **106**, 2316.
19 J. Krijn and E. J. Baerends, in *Fit Functions in the JFS Method*, (in Dutch), Free University of Amsterdam, Amsterdam, 1984.
20 S. D. Vosko, L. Wilk and M. Nusair, *Can. J. Phys.*, 1990, **58**, 1200.
21 (*a*) C. Amatore, M. Azzali and A. Jutand, *J. Organomet. Chem.*, 1989, **363**, C41; (*b*) C. Amatore, M. Azzali and A. Jutand, *J. Am. Chem. Soc.*, 1991, **113**, 8375.
22 I. Gauthron, Y. Mugnier, K. Hierso and P. D. Harvey, *Can. J. Chem.*, in the press.
23 (*a*) L. Manojlovic-Muir, K. W. Muir, B. R. Lloyd and R. J. Puddephatt, *J. Chem. Soc., Chem. Commun.*, 1983, 1336; (*b*) B. R. Lloyd and R. J. Puddephatt, *Inorg. Chim. Acta*, 1984, **90**, L77; (*c*) L. Manojlovic-Muir, K. W. Muir, B. R. Lloyd and R. J. Puddephatt, *J. Chem. Soc., Chem. Commun.*, 1985, 536.
24 B. R. Lloyd, L. Manojlovic-Muir, K. W. Muir and R. J. Puddephatt, *Organometallics*, 1993, **12**, 1231.
25 Host-guest reactivity of $Pd_3(\mu_3\text{-CO})(\mu\text{-dppm})_3^{2+}$ has been observed recently by UV-visible spectroscopy. This reactivity is reversible by bubbling another gas.
26 M. Sakamoto, I. Shimizu and A. Yamamoto, *Organometallics*, 1994, **13**, 407.
27 D. T. Pierce and W. E. Geiger, *J. Am. Chem. Soc.*, 1992, **114**, 6063.
28 (*a*) C. Amatore, L. Nadjo and J. M. Savéant, *Nouv. J. Chim.*, 1979, **3**, 545; (*b*) E. Lamy, L. Nadjo and J. M. Savéant, *J. Electroanal. Chem.*, 1977, **78**, 403; (*c*) C. Amatore and J. M. Savéant, *J. Am. Chem. Soc.*, 1981, **103**, 5021; (*d*) C. Amatore, L. Nadjo and J. M. Savéant, *Nouv. J. Chim.*, 1984, **8**, 565.
29 See for example: (*a*) G. R. Lee, J. M. Maher and N. J. Cooper, *J. Am. Chem. Soc.*, 1987, **109**, 2956; (*b*) G. Fachinetti, C. Floriani, A. Chiesi-Villa and C. Guastini, *J. Am. Chem. Soc.*, 1979, **101**, 1767; (*c*) J. Chatt, M. Kubota, G. J. Leigh, T. C. March, R. Mason and D. J. Yarrow, *J. Chem. Soc., Chem. Commun.*, 1974, 1033; (*d*) H. H. Karsch, *Chem. Ber.*, 1977, **110**, 2213; (*e*) E. Carmona, F. Gonzalez, M. L. Poveda and J. M. Marin, *J. Am. Chem. Soc.*, 1983, **105**, 3365; (*f*) R. Alvarez, E. Carmona, M. L. Poveda and R. Sanchez-Delgado, *J. Am. Chem. Soc.*, 1984, **106**, 2731.
30 R. H. Crabtree, *The Organometallic Chemistry of the Transition Metals*, Wiley, New York, 2nd edn., 1994, p. 318.
31 D. H. Gibson, *Chem. Rev.*, 1996, **96**, 2063.
32 W. Leitner, *Coord. Chem. Rev.*, 1996, **153**, 257.
33 M. Aresta, C. F. Nobile, V. G. Albano, E. Forni and M. Manassro, *J. Chem. Soc., Chem. Commun.*, 1975, 636.
34 T. Heckovitz, *J. Am. Chem. Soc.*, 1977, **99**, 2391.
35 E. Kaufmann, S. Sieber and P. von Ragué Schleyer, *J. Am. Chem. Soc.*, 1989, **111**, 4005.
36 S. Sakaki and K. Ohkubo, *Inorg. Chem.*, 1988, **27**, 2020.
37 S. Sakaki and Y. Musashi, *J. Chem. Soc., Dalton Trans.*, 1994, 3047.
38 C. Bo and A. Dedieu, *Inorg. Chem.*, 1989, **28**, 304.
39 M. Sodupe, V. Branchadell and A. Oliva, *J. Phys. Chem.*, 1995, **99**, 8567.
40 S. Sirois, M. Castro and D. R. Salahub, *Int. J. Quantum Chem.: Quantum Chem. Symp.*, 1994, **28**, 645.
41 R. Provencher and P. D. Harvey, *Inorg. Chem.*, 1996, **35**, 2113.
42 P. D. Harvey, R. Provencher, J. Gagnon, T. Zhang, D. Fortin, K. Hierso, M. Drouin and S. M. Socal, *Can. J. Chem.*, 1996, **74**, 2268.
43 F. A. Cotton, G. Wilkinson and P. D. Gaus, *Basic Inorganic Chemistry*, Wiley, Toronto, 3rd edn., 1995, p. 61. The covalent radii for Ni is 1.25 Å.
44 We estimate the covalent radii for Pd to be ≈1.32 Å, which is half of the average of all known Pd—Pd bond distances for singly bonded dimers. See, for example: P. D. Harvey and Z. Murtaza, *Inorg. Chem.*, 1993, **32**, 4721.
45 M. J. Fink, J. T. Mague and Y. Pan, *J. Am. Chem. Soc.*, 1993, **115**, 3842.
46 For a recent review see: P. D. Harvey, *J. Cluster Sci.*, 1993, **4**, 377.
47 P. D. Harvey, R. F. Dallinger, W. H. Woodruff and H. B. Gray, *Inorg. Chem.*, 1989, **28**, 3057.
48 P. D. Harvey and H. B. Gray, *J. Am. Chem. Soc.*, 1988, **110**, 2145.
49 R. V. Kirss and R. Eisenberg, *Inorg. Chem.*, 1989, **28**, 3372.
50 S. Sakaki, M. Ogawa and Y. Musashi, *J. Phys. Chem.*, 1995, **99**, 17134.

Received 3rd *February* 1997; *revised M/S received* 23rd *June* 1997; *Paper* 7/08331I